EDGE ARTICLE

Check for updates

Coordination modulated on-off switching of flexibility in a metal–organic framework†

Jorge Albalad, [iD] [a] Ricardo A. Peralta, [a] Michael T. Huxley, [a] Steven Tsoukatos, [a] Zhaolin Shi, [b] Yue-Biao Zhang, [iD] [b] Jack D. Evans, [iD] ‡[c] Christopher J. Sumby [iD] *[a] and Christian J. Doonan [iD] *[a]

Stimuli-responsive metal–organic frameworks (MOFs) exhibit dynamic, and typically reversible, structural changes upon exposure to external stimuli. This process often induces drastic changes in their adsorption properties. Herein, we present a stimuli-responsive MOF, **1**·[CuCl], that shows temperature dependent switching from a rigid to flexible phase. This conversion is associated with a dramatic reversible change in the gas adsorption properties, from Type-I to S-shaped isotherms. The structural transition is facilitated by a novel mechanism that involves both a change in coordination number (3 to 2) and geometry (trigonal planar to linear) of the post-synthetically added Cu(I) ion. This process serves to 'unlock' the framework rigidity imposed by metal chelation of the bis-pyrazolyl groups and realises the intrinsic flexibility of the organic link.

Introduction

Metal–organic frameworks (MOFs) are a class of network solids that have been widely explored for their potential applications in gas storage[1–4] and separations.[5–7] These research efforts have demonstrated that MOFs can exhibit unique, and typically reversible, structural flexibility that can result in dynamic adsorption properties.[8–12] For example, Fe(bdp) and Co(bdp) (bdp = 1,4-benzenedipyrazolate) show pressure dependent adsorption of methane that is associated with a reversible transition between collapsed and expanded phases.[13] Another remarkable case is DUT-49, which undergoes a structural transformation that yields a 50% reduction in the unit cell volume resulting in negative gas adsorption.[10,14]

Structural modes of flexibility observed in MOFs include breathing, swelling, linker rotation and subnetwork displacement.[15] Typically, these processes are triggered by gas adsorption and desorption phenomena[16–18] but can also be induced by temperature,[19] mechanical pressure,[20] and light.[21,22] Indeed,

such external stimuli have been employed to control the gas adsorption properties of flexible frameworks; examples include molecular sieving of CO_2/N_2 and CO_2/CH_4, which could be realised *via* mechanical pressure in MIL-53,[23] and incorporation of photoswitchable azo-benzene units into the MOF backbone of PCN-123, which is isostructural with MOF-5, to modify its CO_2 adsorption properties.[24] Temperature can also drastically affect the structure of flexible MOFs, for example, inducing significant structural expansion and reversible ion capture.[25,26] These studies highlight that the novel adsorption characteristics of flexible MOFs are determined by the structural origin of flexibility and the type of stimulus. Thus, uncovering new mechanisms that engender reversible phase transitions will expand this area of MOF chemistry and broaden the scope of potential applications.[27]

Work in our laboratory has shown that a manganese(II)-based MOF, **1** ([Mn_3(L)_2L']), where L = L' = bis(4-carboxyphenyl-3,5-dimethyl-pyrazol-1-yl)methane, and L' possesses a free *N,N'* chelating site) can retain crystallinity following post-synthetic metalation and consecutive chemical reactions at the extraneous metal site.[28–32] We have shown that this is primarily due to the intrinsic flexibility of the organic linker which alleviates strain on the framework caused by changes in geometry of the chelated metal ion during reactions.[33] A salient example is cobalt(II) metalated **1** which undergoes a reversible, temperature-dependent, conversion between octahedral **1**·[Co(H_2O)_4]Cl_2 and tetrahedral **1**·[CoCl_2] geometries at the post-synthetic metalation site (Fig. 1).[28] These previous observations prompted us to investigate whether coordination chemistry could be exploited as a novel strategy to achieve stimuli-responsive flexibility in **1**. With this in mind, we chose to

[a]Centre for Advanced Nanomaterials and Department of Chemistry, The University of Adelaide, North Terrace, Adelaide, SA 5000, Australia. E-mail: christopher.sumby@adelaide.edu.au; christian.doonan@adelaide.edu.au

[b]School of Physical Science and Technology, ShanghaiTech University Shanghai, 201210, China

[c]Department of Inorganic Chemistry, Technische Universität Dresden, 01062 Dresden, Germany

‡ Present address for J. D. E.: Centre for Advanced Nanomaterials and Department of Chemistry, The University of Adelaide, Adelaide, South Australia 5000, Australia.
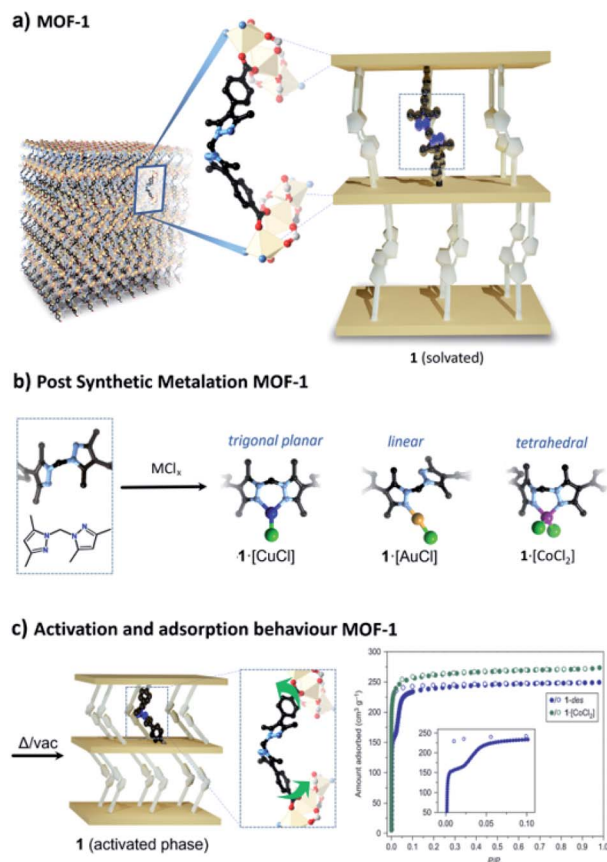
Fig. 1 (a) A key feature of MOF **1** is the flexible organic linker which bridges sheets of Mn(II) trimers; this structural element has been simplified into a schematic representation to aid the reader. (b) Free N,N'-chelation sites in **1** readily undergo post-synthetic metalation with transition metal salts and complexes including CuCl, AuCl(dms) (dms = dimethylsulfide) and CoCl$_2$. (c) To provide some context to the studies reported, we note that activation of MOF **1** leads to contraction of the framework due to the flexibility of the non-metalated bridging linker; this manifests in the 77 K N$_2$ isotherm in the form of a pronounced inflexion (filled circles represent adsorption and open circles represent desorption data points).[26] Notably, the inflexion is absent when the material is metalated with CoCl$_2$, which imparts rigidity into the bridging linker (C, black; N, pale blue; Cu, orange; Cl, green; Au, yellow; Co, pink).

linear) of the post-synthetically added Cu(I) ion which serves to 'unlock' the rigidity imposed by chelation of the bis-pyrazolyl group. Given the tailorable synthesis of MOFs and vast number of coordination complexes that are known, we believe that this work provides general design principles for the synthesis of stimuli-responsive flexible MOF materials.

Results and discussion

1·[CuCl] was synthesised by immersing single crystals of **1** in a solution of CuCl in acetonitrile. Single crystal X-ray diffraction (SCXRD) revealed that the metalated product, **1**·[Cu(MeCN)Cl], is a mixture of disordered tetrahedral Cu(I) centres; an ionic bis-acetonitrile [Cu(MeCN)$_2$]Cl and a neutral [Cu(MeCN)Cl] species.[30] Washing the crystals with non-polar solvents (e.g. toluene, diethyl ether, or alkanes) drives the quantitative formation of the non-solvated, trigonal planar species, **1**·[CuCl] (Fig. 1). Conversion of the disordered tetrahedral species to a well-defined trigonal planar complex was confirmed by SCXRD data, which revealed a porous framework of $V_{cell}/Z = 2677.6$ Å^3, with a Cu–Cl bond distance of 2.203(4) Å, commensurate with other literature examples (Fig. S1 and S2†).[36–38]

We assessed the adsorption properties of **1**·[CuCl] by performing 77 K N$_2$ adsorption isotherms. Sample activation from n-pentane at 100 °C gave rise to an adsorption profile that showed negligible N$_2$ uptake until $P/P_0 = 0.3$ followed by steep uptake of N$_2$ to a maximum value of 150 cm^3 g^{-1} and a hysteretic desorption (Fig. 2 and S3a†). The features of this isotherm

metalate **1** with Cu(I) as it exhibits diverse low coordinate geometries (e.g. 2 (linear), 3 (trigonal planar) and 4 (tetrahedral) are known)[34] that can be interconverted under carefully controlled conditions.[30,35] In addition, we recently demonstrated that **1** can support both tetrahedral and trigonal planar geometries for Cu(I).[30] Thus, we speculated whether a flexible MOF material could be realised by modulating the Cu(I) coordination geometry, i.e. switching from a rigid framework (Cu(I) is chelated) to a flexible framework (Cu(I) is monodentate).

Here we report the temperature dependent switching of **1**·[CuCl] from a rigid to flexible system. This conversion is associated with a dramatic change in the gas adsorption properties that show Type-I and S-shaped isotherms for the rigid and flexible forms, respectively. The novel mechanism underpinning this structural transformation involves a change in coordination number (3 to 2) and geometry (trigonal planar to
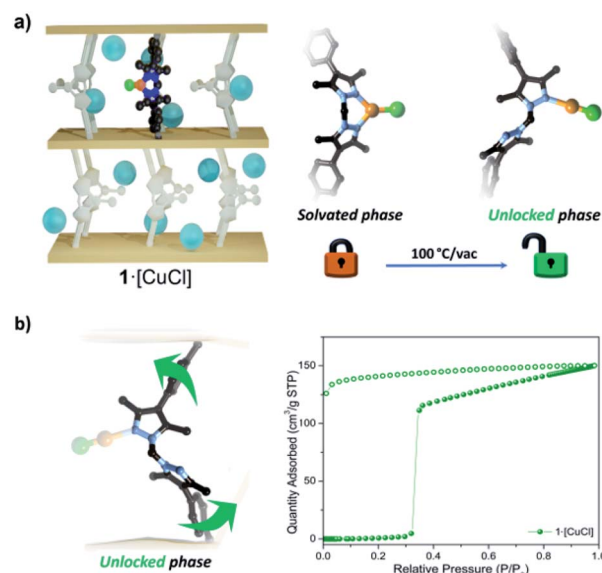

Fig. 2 (a) Schematic representation of the principal processes associated with the activation of **1**·[CuCl] under 100 °C per vacuum conditions, that lead to framework contraction due to the formation of a linear, 'unlocked' N–CuCl site which allows the MOF to access the intrinsic flexibility of the organic linker. (b) 77 K N$_2$ adsorption isotherm of **1**·[CuCl]-unlocked after activation under vacuum from n-pentane at 100 °C for 90 minutes. A clear gate-opening effect is observed due to the inherent flexibility of the digonal complex, giving the isotherm an S-shaped profile characteristic of flexible frameworks.

are typical for flexible MOF materials where a pressure-induced transition yields an enhancement in accessible surface area.[39] In addition, we activated 1·[CuCl] from different dry solvents, including methanol, acetone, and diethyl ether. Interestingly, although the isotherms obtained from these solvents show an analogous profile, the gate opening pressure is shifted to P/P_0 = 0.1 (Fig. S4†). We attribute this phenomena to the presence of residual solvent molecules trapped within the collapsed framework upon activation that can lower the activation energy for phase transitions.[40] This hypothesis is supported by TGA-MS measurements performed on activated samples of 1·[CuCl] showing residual solvent (Fig. S5 and S6†). It is noteworthy that dynamic adsorption behaviour is also observed for non-metalated 1, where a gate-opening event takes place at very low pressure (P/P_0 = 0.025) producing an inflexion in the isotherm (Fig. 1c). This step originates from the intrinsic flexibility of the bridging linker which, when not metalated, is free to rotate during activation and, allows for the framework pores to collapse. This process has been previously elucidated from SCXRD data obtained from activated crystals of 1 (Fig. 1).[28] The pronounced step observed in the 77 K N_2 isotherm of 1·[CuCl] suggests that during activation the framework undergoes a structural transition from the open solvated phase to a closed phase. We hypothesised that this transformation is facilitated by a change in coordination geometry around the Cu(I) centre from trigonal planar to digonal, which unlocks the ligand flexibility and triggers the formation of the collapsed, 1·[CuCl]-unlocked, phase (Fig. 2). We note that Cu(I) complexes are known to readily access a digonal geometry.[35,41–48] Indeed, density functional theory (DFT) calculations performed on representative molecular subunits reveal that there is a slight energetic preference for the digonal 1·[CuCl]-unlocked over the trigonal planar 1·[CuCl] species (~5 kJ mol^{-1}). However, for the analogous Br and I species, the trigonal planar coordination is thermodynamically favoured (Fig. S7 and S8†). We examined 1·[CuCl] via Raman spectroscopy to ascertain if there are structural differences between as-synthesised and 1·[CuCl]-unlocked. The spectra show clear and non-reversible changes, suggesting that a different, thermodynamically-favoured Cu(I) geometry is formed during thermal activation, and is retained throughout the subsequent isotherm (Fig. S9 and S10†). To gain further insight into the 1·[CuCl]-unlocked phase we performed SCXRD experiments using a synchrotron X-ray source. The resulting diffraction data was solved in the space group $P\bar{1}$ with a unit cell volume per formula unit (V_{cell}/Z) of 2148.5 Å^3 (20% volume decrease from 1·[CuCl]). This volume is notably similar to those obtained from the structure of, non-metalated, 1 (V_{cell}/Z = 2174.7 Å^3).[28] Refinement of the structure showed that the bis-pyrazolyl sites of the bridging linker clearly adopt an 'anti' configuration which is consistent with the hypotheses that the closed phase is digonal. However, due to positional disorder, we were unable to resolve the coordination environment of the Cu(I) centre (Fig. S11 and S12†). Nonetheless, based on the collapsed structure observed, the coordinated [Cu–Cl] would be in close proximity to neighbouring framework atoms and such interactions would stabilise the closed structure, consistent with the higher gate-opening pressure observed compared to

non-metalated 1. To confirm that Cu(I) is retained in the conversion from 1·[CuCl] to 1·[CuCl]-unlocked we carried out energy-dispersive X-ray spectroscopy (EDX). The resulting data afforded the expected ratio Mn : Cu : Cl ratio of 3 : 1 : 1 (Table S1†). Furthermore, we examined samples of the 1·[CuCl]-unlocked via transmission electron microscopy (TEM) and found no evidence that the Cu(I) ions had migrated from the coordinating linker to form nanoparticles (Fig. S14†).

Next, we compared the 77 K N_2 adsorption profile of 1·[CuCl]-unlocked to two sets of control samples: (i) a bonafide digonal complex 1·[AuCl]; and (ii) 1·[CuBr] and 1·[CuI] that, according to previously discussed DFT simulations, show a thermodynamic preference for the trigonal planar geometry (Fig. S7 and S8†). 1·[AuCl] was synthesised by metalating 1 with [AuCl(dms)] (dms = dimethylsulfide) in diethyl ether, a solvent known to favour the 'anti' conformation at the N,N'-coordination site.[33] SCXRD analysis revealed a linear AuCl complex coordinated to a single N-donor site in 1 (Fig. 1, Fig. S15 and S16†), and EDX analysis of the crystals (Table S2 and Fig. S17†)
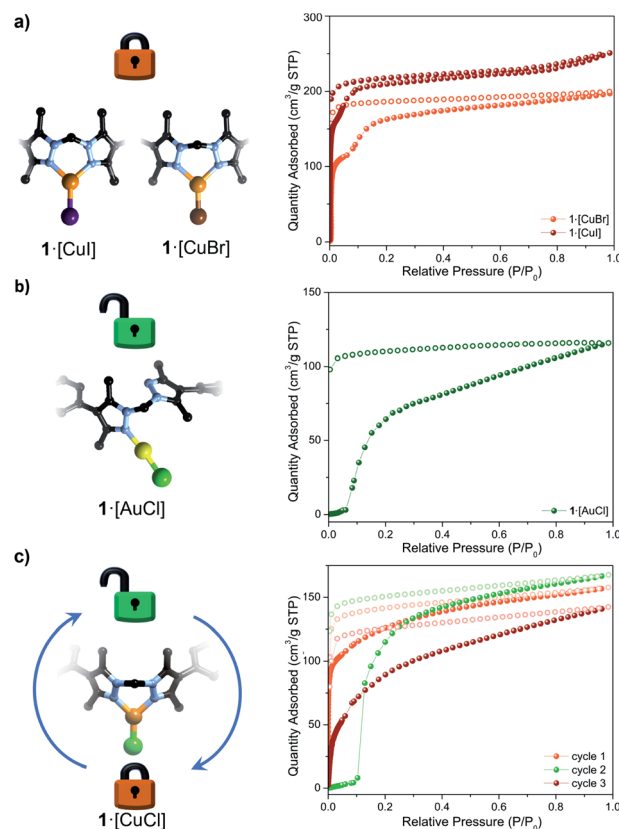

Fig. 3 (a) 77 K N_2 adsorption isotherm of 1·[CuBr] (orange) and 1·[CuI] (dark red) under 100 °C/vacuum activation conditions, that maintain their trigonal planar conformation and act as 'permanently-locked' control samples. (b) 77 K N_2 adsorption isotherm of the 'permanently-unlocked' 1·[AuCl] sample activated at room temperature, which allows the MOF to access the intrinsic flexibility of the organic linker. (c) 77 K N2 3-cycle adsorption isotherm of 1·[CuCl] after activation under mild conditions, then heated at 100 °C for 90 minutes, and finally resolvated and reactivated under mild conditions. A clear gate-opening effect is observed after heating, giving the isotherm an S-shaped profile characteristic of flexible frameworks.

confirmed the expected Mn : Au : Cl ratio of 3 : 1 : 1. Samples of **1**·[AuCl] were activated at room temperature from diethyl ether and *n*-pentane prior to performing a N$_2$ 77 K adsorption isotherm. The S-type adsorption profile of **1**·[AuCl] (Fig. 3b and S18†) was analogous to that of **1**·[CuCl]-*unlocked*, showing a gate-opening step at $P/P_0 = 0.1$. This data suggests that the adsorption behaviour of **1**·[CuCl]-*unlocked* is consistent with a digonal **1**·[CuCl] species.

Metalation of **1** with CuBr and CuI directly yielded structurally ill-defined multinuclear species within the MOF. To overcome this issue, we employed anion metathesis of **1**·[CuCl] with NaBr or NaI in dry methanol for 24 and 48 hours, respectively.[29,30] In both cases, EDX analysis of the crystals indicated that quantitative halide exchange had occurred (see Mn : Cu : X 3 : 1 : 1 ratios; X = Br, I; Table S3 and Fig. S20†). Single crystal quality for the bromide and iodide exchanged MOFs was excellent, permitting their examination by SCXRD. In both instances, a trigonal planar Cu(I)-halide complex was observed (Fig. 3), with Cu–X bond lengths of 2.268(3) and 2.455(6) Å for the bromide and iodide derivatives, respectively (Fig. S21–S24†). We note that trigonal planar halide complexes of Cu(I) are rare,[49] and these results present an unusual example in which three halide species are accessible *via* simple solvent and anion exchange chemistry within a MOF matrix. 77 K N$_2$ isotherms were collected on samples of **1**·[CuBr] and **1**·[CuI] under the same activation conditions employed for **1**·[CuCl]-*unlocked*. **1**·[CuBr] and **1**·[CuI] exhibit Type-I-like profiles that are consistent with a 'locked' trigonal planar conformer (S_{BET} = 492 m^2 g^{-1} for **1**·[CuBr], 727 m^2 g^{-1} for **1**·[CuI], Fig. 3a, S25 and S26†). Both isotherms display an inflexion shoulder after the microporous region attributed to conformational freedom at the trigonal planar sites.[50] The combined structural and gas adsorption data (*vide supra*) of the control samples suggests that in the activated phase Cu(I) adopts a linear conformation subsequent to thermal activation and that the gate-opening phenomena is due to the underlying flexibility of organic link coordinating in a monodentate fashion.

Two sought after properties of flexible MOF materials are reversible gas adsorption and on/off porosity switching.[18,51,52] Thus, we investigated if the activated phases **1**·[CuCl]-*locked*

(trigonal planar) and **1**·[CuCl]-*unlocked* (digonal) could be accessed independently, and if the transition from a rigid to flexible phase could be triggered *in situ* by an external stimulus (Fig. 4). Given that DFT studies indicate a low energy barrier for the conversion of trigonal planar **1**·[CuCl] to a digonal **1**·[CuCl], we thought that mild activation conditions may allow for **1**·[CuCl]-*locked* to be isolated, and its gas adsorption properties examined. Samples of **1**·[CuCl] activated at room temperature from either diethyl ether or *via* supercritical CO$_2$ were assessed by 77 K N$_2$ gas adsorption isotherms (Fig. S28†). In both instances, the isotherm profiles were Type-I S_{BET} surface area values of 565 m^2 g^{-1} (ether activation) and 441 m^2 g^{-1} (scCO$_2$ activation), and show an analogous shoulder to the trigonal planar **1**·[CuI] and **1**·[CuBr] species, albeit less pronounced. Remarkably, following activation, the crystals remained in excellent condition allowing for their structures to be determined using SCXRD. Analysis of the diffraction data afforded the expected trigonal planar geometry for the Cu(I) ion, with no crystallographically defined solvent molecules within the MOF pores (Fig. S30 and S31†). Next, we explored the potential switching from the open to the closed phase of the MOF *in situ*. After collecting an isotherm on the open phase, the sample was heated at 100 °C for 90 min. A second 77 K N$_2$ isotherm was then carried out on the heated sample, showing a drastic change in the isotherm profile; from Type-I to the S-type profile characteristic of **1**·[CuCl]-*unlocked* (Fig. 3c). Lastly, this same sample of **1**·[CuCl]-*unlocked* was re-solvated *via* immersion of the material in dry MeCN. This process led to the recovery of the initial tetrahedral complex, **1**·[Cu(MeCN)Cl] (referred hereafter as **1**·[CuCl]-*resolv* for clarity, Fig. S32 and S33†). This sample was activated, either after washing with diethyl ether at room temperature or supercritical CO$_2$, and a third N$_2$ isotherm was performed at 77 K after recovering the trigonal planar conformation. As expected, a non-gated adsorption profile was observed again for both samples, although slightly reduced S_{BET} values were recorded (S_{BET} = 292 m^2 g^{-1} (ether), 264 m^2 g^{-1} (scCO2); Fig. 3c and S32†). We attribute this reduction of surface area and total uptake values to slight structural degradation upon the three solvent-exchange-activation-isotherm measurement cycles.
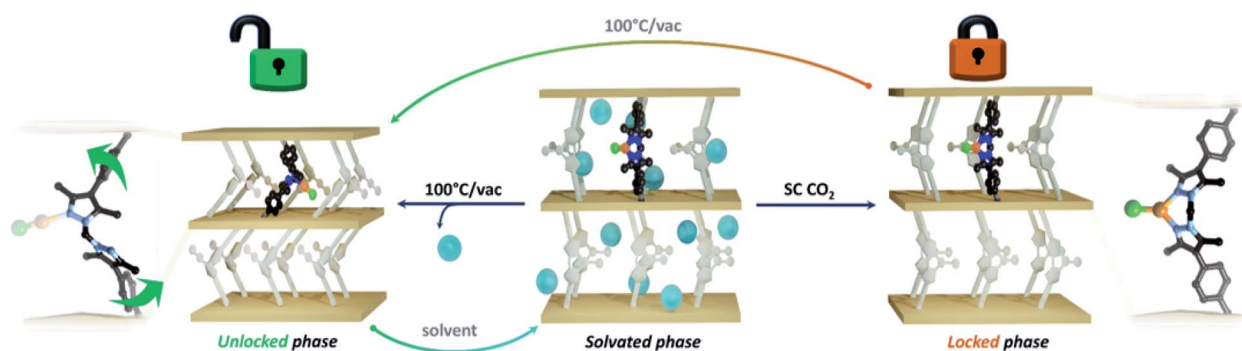

Fig. 4 Schematic representation of the principal processes associated with the activation of **1**·[CuCl] under mild (SC CO$_2$) and harsh (100 °C per vacuum) conditions. Mild conditions lead to an open 'locked' framework with trigonal planar geometry retained at the *N,N′*-CuCl sites while harsher conditions lead to framework contraction due to the formation of a linear, 'unlocked' *N*-CuCl site which allows the MOF to access the intrinsic flexibility of the organic linker in a reversible fashion.

Conclusions

In summary, we have uncovered a new mechanism for realising structural flexibility in MOFs that allows for control of the bulk material adsorption properties. Due to the mutable coordination chemistry of Cu(I), **1**·[CuCl] can be isolated as a rigid, trigonal planar **1**·[CuCl]-*locked*, or flexible, digonal **1**·[CuCl]-*unlocked* species by careful choice of activation conditions. These materials engender distinct gas adsorption characteristics; **1**·[CuCl]-*locked* affords a Type-I isotherm typical of a rigid microporous material while **1**·[CuCl]-*unlocked* yields an S-shaped isotherm profile that is characteristic of flexible MOFs. Furthermore, heating samples of **1**·[CuCl]-*locked* triggers a structural transition to **1**·[CuCl]-*unlocked*, providing a simple approach to stimuli-induced on-off porosity switching. Likewise, re-solvating **1**·[CuCl]-*unlocked* recovers the initial complex, and consequently, the rigidity of the material. Throughout these phase transitions crystallinity was retained, permitting structural elucidation of each step *via* SCXRD, and thus providing deep insight into the mechanism underlying these transformations. We believe that coordination-modulated flexibility could be employed to design new MOF materials that are composed of intrinsically flexible linkers that can coordinate transition metals. In addition, such materials could show desirable performance characteristics for application to areas such as molecular sensing.

Experimental section

Materials and methods

All reagents were obtained from commercial sources and used without further purification. Unless otherwise stated, all reactions and sample handling were performed under an argon atmosphere using standard Schlenk techniques. Solvents were dried and distilled using literature procedures and degassed with Ar prior to use. Specifically, acetonitrile (MeCN) was dried from CaH_2 under N_2; methanol was dried by refluxing over Mg beads under N_2 followed by distillation and storage over 4 Å molecular sieves; acetone was dried and distilled from $CaSO_4$ under N_2; and pentane, cyclohexane, toluene and diethyl ether were dried over Na/benzophenone. NaBr and NaI used for anion exchange were stored in a 120 °C drying oven. **1**·[AuCl] is light-sensitive and must be handled and stored accordingly.

Characterisation

SEM imaging and Energy-Dispersive X-ray (EDX) spectroscopy data were collected using a Philips XL30 field-emission scanning electron microscope (FESEM) operating at 20.00 kV. TEM images were collected on a FEI Tecnai G2 Spirit microscope. The samples were sonicated in dry methanol for 20 minutes to ensure a good delamination of the crystals and improve the overall dispersibility. Thermogravimetric analysis (TGA) of activated **1**·[CuCl]-*unlocked* from diethyl ether and *n*-pentane were collected on a Netzsch STA449 F3 Jupiter + QMS403 Aeolos® Quadro thermogravimetric analyser, coupled to

a Mass-Spectrometry detector fixed at MW = 72 (pentane) and 74 (diethyl ether).

Raman spectroscopy

Raman spectrum was collected using an alpha300 RS from WITec with activated sample sealed in a glove box under N_2 atmosphere. The excitation wavelength was 532 nm, integration time was 120 s with 4 times of accumulations, the grating is G3 1200 g mm^{-1} (BLZ = 500 nm). Two equivalent batches of as-synthesised **1**·[CuCl] were transferred to two different Raman sample cells (see Fig. S9†) within a globe box. The former (Cell#1) was left undisturbed, while the latter (Cell#2) was activated under temperature and vacuum for 8 hours to ensure a complete conformational change. The Raman spectra of both cells were then collected before running an *in situ* N_2 adsorption isotherm at 77 K on the activated sample. A final Raman spectrum, post-isotherm, was then collected to spot any potential conformational change during the desorption step.

Gas sorption measurements

Gas adsorption isotherms (77 K N_2, 195 K CO_2) were measured on a Micromeritics 3-flex Surface Area Analyser, and on an ASAP 2020 Surface Area and Pore Size Analyser. Unless otherwise specified, wet crystals of **1** were loaded under argon to the adsorption cell, and the final mass was corrected after the isotherm data collection. Specific activation conditions are described in the main text and in the caption text of the corresponding ESI figures.†

Single crystal and powder X-ray diffraction

Single crystals were mounted in paratone-N oil on a nylon loop. SCXRD data for **1**·[Cu(MeCN)Cl],[30] **1**·[CuCl], **1**·[CuCl]-*locked*, **1**·[CuCl]-*unlocked*, **1**·[CuCl]-*resolv*, **1**·[CuBr], **1**·[CuI], and **1**·[AuCl] were collected at 100 K on the MX1 or MX2 beamlines of the Australian Synchrotron using the BluIce software interface,[53] operating at $\lambda = 0.7108$ Å. Single crystal X-ray data for **1**·[CuCl] was collected at 150(2) K on an Oxford X-Calibur single crystal diffractometer ($\lambda = 0.71073$ Å). N_{tot} reflections were merged to N unique (R_{int} quoted) after a multi-scan absorption correction (proprietary software) and used in the full matrix least squares refinements on F^2. Unless otherwise stated in the additional refinement details, anisotropic displacement parameter forms were refined for the non-hydrogen atoms; hydrogen atoms were treated with a riding model [weights: $(\sigma 2(F_o)^2 + (aP)^2 + (bP))^{-1}$; $P = (F_o{}^2 + 2Fc^2)/3$]. Neutral atom complex scattering factors were used; computation used the SHELXL program.[54] Pertinent results are given in the manuscript, while views of the asymmetric units, additional refinement details, and X-ray experimental and refinement data (Table S3 and Fig. S9–S22†) are given in the ESI.† Full details of the structure determinations have been deposited with the Cambridge Crystallographic Data Centre as CCDC #s 2100590–2100596.†

Powder X-ray diffraction data was collected on a Bruker Advance D8 diffractometer equipped with a capillary stage using Cu Kα radiation ($\lambda = 1.5418$ Å). Simulated powder X-ray diffraction (PXRD) patterns were produced from the single

crystal data using Mercury Software. **1**·[CuCl]-*unlocked* PXRD was collected after activating the sample under vacuum at 100 °C for 90 min inside a Pyrex capillary, flame sealed under vacuum prior to the measurement.

DFT simulations

A representative molecular model of the framework, as used in a previous study,[29] where the framework was cleaved at the pyrazole C4 position and capped with methyl functionality was employed to investigate the coordination of bis-pyrazole system. Geometry optimizations of this molecule coordinated to a Cu centre with a series of halogens (Cl, Br, I) in either a two or three-coordinate conformation used the PBE0 density functional[55] employed by the ORCA software package.[56,57] The polarized triple-zeta basis set def2-TZVP[58] was used and tight SCF convergence criteria were implemented to obtain reliable accuracy. Dispersion corrections (D3-BJ) were also applied.[59] Further information is detailed in ESI (see Fig. S7 and S8†) and representative data files are available online in the data repository https://github.com/jackevansadl/supp-data.

Synthetic procedures

H₂L. The ligand bis(4-(4-carboxyphenyl)-1*H*-3,5-dimethylpyrazolyl)methane (H₂L) was synthesized following a previously reported procedure.[28]

1. Single crystals of **1** were prepared as previously reported.[28] Briefly, 31.6 mg of H₂L and 24.2 mg of $MnCl_2 \cdot 4H_2O$ were dissolved in 6 mL of a DMF : H₂O mixture (2 : 1 v/v). The solution was transferred to a scintillation vial and heated at 100 °C for 48 h. The as-obtained colourless plate-shaped crystals were washed with DMF (3 × 10 mL) and kept under solvent prior to their use.

1·[Cu(MeCN)Cl]. Single crystals of **1** (~24 mg) were placed in a 4 mL glass vial and washed with freshly distilled acetonitrile (5 × 5 mL) under Ar flow (the solution was degassed with Ar after each exchange, and the sample was allowed to soak for 1 h between washings). CuCl (30 mg) was added and the vial was sealed under Ar and left undisturbed at 4 °C for 72 h. The resulting yellow crystals were washed with freshly distilled acetonitrile (5 × 5 mL) and stored under Ar.

1·[CuCl]. Crystals of **1**·[CuCl(MeCN)] were washed under Ar flow with freshly distilled MeOH (5 × 5 mL), acetone (5 × 5 mL) and a non-polar solvent (toluene, *n*-pentane, cyclohexane) (5 × 5 mL) allowing the sample to soak for 1 h in between washings.

1·[CuCl]-*locked*. Crystals of **1**·[CuCl] were washed in Et₂O (5 × 5 mL) allowing the sample to soak for 1 h between washings. The sample was then activated under dynamic vacuum for 90 min at room temperature and backfilled with Argon.

1·[CuCl]-*unlocked*. Crystals of **1**·[CuCl] were slowly activated under dynamic vacuum (pressure slope: −10 mbar min⁻¹) in an adsorption cell and then heated at 100 °C for 2 hours after reaching full vacuum.

1·[CuCl]-*resolv*. Crystals of **1**·[CuCl]-*unlocked* were backfilled with Argon and soaked in dry acetonitrile for 2 hours.

1·[AuCl]. Single crystals of **1** (~24 mg) were placed in a cellulose filter within a 4 mL glass vial and washed with freshly

distilled Et₂O (5 × 5 mL) under Ar flow (the solution was degassed with Ar after each exchange, and the sample was allowed to soak for 1 h between washings). AuCl(dms) (dms = dimethylsulfide) (10 mg) was added to the ether phase and the vial was sealed under Ar and left under stirring in the dark at room temperature for 48 h. The resulting pale-yellow crystals were taken out of the filter, washed with freshly distilled Et₂O (5 × 5 mL) and stored under Ar in the dark.

Anion exchange protocol for 1·[CuBr] and 1·[CuI]. Crystals of **1**·[CuCl] were soaked in dry methanol. Dry NaBr or NaI (~100 mg) was then loaded to a small glass ampule and subsequently submerged in the 4 mL vial containing the MOF sample. The solution was degassed with Ar, and the vial was sealed and allowed to stand at room temperature for 24 h or 48 h, respectively. Under Ar flow, the ampule containing undissolved salt was removed and the resulting brown crystals were washed with freshly distilled methanol (5 × 5 mL), acetone (5 × 5 mL) and *n*-pentane (5 × 5 mL).

Data availability

Representative data files for computational calculations are available online in the data repository https://github.com/jackevansadl/supp-data.

Author contributions

J. A. and C. J. D. conceived the project. J. A., R. A. P. and M. T. H. performed all the synthesis, characterisation, and SCXRD data collection for all the **1**·[CuX] (X= Cl, Br, I) samples. S. T. synthesised and characterised **1**·[AuCl]. Z. S. and Y.-B. Z. carried out the *in situ* Raman spectroscopy, and provided all the equipment for the measurements. J. D. E. performed the computational calculations. C. J. S. refined all the SCXRD data. J. A., M. T. H. and C. J. D. prepared the final manuscript and ESI. C. J. S. and C. J. D. supervised this work and acquired the financial support for the project. All authors collectively discussed the results, provided insightful inputs, and peer-reviewed the manuscript prior to submission.

Conflicts of interest

There are no conflicts to declare.

Acknowledgements

Notes and references

1 J. E. Bachman, M. T. Kapelewski, D. A. Reed, M. I. Gonzalez and J. R. Long, *J. Am. Chem. Soc.*, 2017, **139**, 15363–15370.

2 M. P. Suh, H. J. Park, T. K. Prasad and D.-W. Lim, *Chem. Rev.*, 2012, **112**, 782–835.

3 H. Wu, Q. Gong, D. H. Olson and J. Li, *Chem. Rev.*, 2012, **112**, 836–868.

4 E. Mahmoud, *J. Porous Mater.*, 2021, **28**, 213–230.

5 K. Adil, Y. Belmabkhout, R. S. Pillai, A. Cadiau, P. M. Bhatt, A. H. Assen, G. Maurin and M. Eddaoudi, *Chem. Soc. Rev.*, 2017, **46**, 3402–3430.

6 Z. Bao, G. Chang, H. Xing, R. Krishna, Q. Ren and B. Chen, *Energy Environ. Sci.*, 2016, **9**, 3612–3641.

7 H. Li, K. Wang, Y. Sun, C. T. Lollar, J. Li and H.-C. Zhou, *Mater. Today*, 2018, **21**, 108–121.

8 B. Mu, F. Li, Y. Huang and K. S. Walton, *J. Mater. Chem.*, 2012, **22**, 10172–10178.

9 J. Rogacka, F. Formalik, A. L. Triguero, L. Firlej, B. Kuchta and S. Calero, *Phys. Chem. Chem. Phys.*, 2019, **21**, 3294–3303.

10 S. Krause, V. Bon, I. Senkovska, U. Stoeck, D. Wallacher, D. M. Többens, S. Zander, R. S. Pillai, G. Maurin, F.-X. Coudert and S. Kaskel, *Nature*, 2016, **532**, 348–352.

11 L. R. Parent, C. H. Pham, J. P. Patterson, M. S. Denny, S. M. Cohen, N. C. Gianneschi and F. Paesani, *J. Am. Chem. Soc.*, 2017, **139**, 13973–13976.

12 H. J. Choi, M. Dincă and J. R. Long, *J. Am. Chem. Soc.*, 2008, **130**, 7848–7850.

13 J. A. Mason, J. Oktawiec, M. K. Taylor, M. R. Hudson, J. Rodriguez, J. E. Bachman, M. I. Gonzalez, A. Cervellino, A. Guagliardi, C. M. Brown, P. L. Llewellyn, N. Masciocchi and J. R. Long, *Nature*, 2015, **527**, 357–361.

14 B. Garai, V. Bon, S. Krause, F. Schwotzer, M. Gerlach, I. Senkovska and S. Kaskel, *Chem. Mater.*, 2020, **32**, 889–896.

15 A. Boutin, F.-X. Coudert, M.-A. Springuel-Huet, A. V. Neimark, G. Férey and A. H. Fuchs, *J. Phys. Chem. C*, 2010, **114**, 22237–22244.

16 R. Pallach, J. Keupp, K. Terlinden, L. Frentzel-Beyme, M. Kloß, A. Machalica, J. Kotschy, S. K. Vasa, P. A. Chater, C. Sternemann, M. T. Wharmby, R. Linser, R. Schmid and S. Henke, *Nat. Commun.*, 2021, **12**, 4097.

17 D. Fairen-Jimenez, S. A. Moggach, M. T. Wharmby, P. A. Wright, S. Parsons and T. Düren, *J. Am. Chem. Soc.*, 2011, **133**, 8900–8902.

18 A. Schneemann, V. Bon, I. Schwedler, I. Senkovska, S. Kaskel and R. A. Fischer, *Chem. Soc. Rev.*, 2014, **43**, 6062–6096.

19 Y. Liu, J.-H. Her, A. Dailly, A. J. Ramirez-Cuesta, D. A. Neumann and C. M. Brown, *J. Am. Chem. Soc.*, 2008, **130**, 11813–11818.

20 K. Yang, G. Zhou and Q. Xu, *RSC Adv.*, 2016, **6**, 37506–37514.

21 R. Lyndon, K. Konstas, B. P. Ladewig, P. D. Southon, P. C. J. Kepert and M. R. Hill, *Angew. Chem., Int. Ed. Engl.*, 2013, **52**, 3695–3698.

22 L. L. Gong, X. F. Feng and F. Luo, *Inorg. Chem.*, 2015, **54**, 11587–11589.

23 N. Chanut, A. Ghoufi, M.-V. Coulet, S. Bourrelly, B. Kuchta, G. Maurin and P. L. Llewellyn, *Nat. Commun.*, 2020, **11**, 1216.

24 J. Park, D. Yuan, K. T. Pham, J.-R. Li, A. Yakovenko and H.-C. Zhou, *J. Am. Chem. Soc.*, 2012, **134**, 99–102.

25 J. Pang, M. Wu, J.-S. Qin, C. Liu, C. T. Lollar, D. Yuan, M. Hong and H.-C. Zhou, *Chem. Mater.*, 2019, **31**, 8787–8793.

26 M. Zhu, X.-Z. Song, S.-Y. Song, S.-N. Zhao, X. Meng, L.-L. Wu, C. Wang and H.-J. Zhang, *Adv. Sci.*, 2015, **2**, 1500012.

27 M. Zhang, M. Bosch, T. Gentle Iii and H.-C. Zhou, *CrystEngComm*, 2014, **16**, 4069–4083.

28 W. M. Bloch, A. Burgun, C. J. Coghlan, R. Lee, M. L. Coote, C. J. Doonan and C. J. Sumby, *Nat. Chem.*, 2014, **6**, 906–912.

29 R. A. Peralta, M. T. Huxley, J. D. Evans, T. Fallon, H. Cao, M. He, X. S. Zhao, S. Agnoli, C. J. Sumby and C. J. Doonan, *J. Am. Chem. Soc.*, 2020, **142**, 13533–13543.

30 R. A. Peralta, M. T. Huxley, J. Albalad, C. J. Sumby and C. J. Doonan, *Inorg. Chem.*, 2021, **60**, 11775–11783.

31 M. T. Huxley, A. Burgun, H. Ghodrati, C. J. Coghlan, A. Lemieux, N. R. Champness, D. M. Huang, C. J. Doonan and C. J. Sumby, *J. Am. Chem. Soc.*, 2018, **140**, 6416–6425.

32 R. A. Perlata, M. T. Huxley, Z. Shi, Y.-B. Zhang, C. J. Sumby and C. J. Doonan, *Chem. Commun.*, 2020, **56**, 15313–15316.

33 R. Peralta, M. Huxley, R. Young, O. M. Linder-Patton, J. D. Evans, C. J. Doonan and C. J. Sumby, *Faraday Discuss.*, 2020, **225**, 84–99.

34 J. M. Muñoz-Molina, T. R. Belderrain and P. J. Pérez, *Coord. Chem. Rev.*, 2019, **390**, 171–189.

35 N. Parvin, J. Hossain, A. George, P. Parameswaran and S. Khan, *Chem. Commun.*, 2020, **56**, 273–276.

36 T. Yoneda, C. Kasai, Y. Manabe, M. Tsurui, Y. Kitagawa, Y. Hasegawa, P. Sarkar and Y. Inokuma, *Chem.–Asian J.*, 2020, **15**, 601–605.

37 D. Anastasiadou, G. Psomas, M. Lalia-Kantouri, A. G. Hatzidimitriou and P. Aslanidis, *Mater. Sci. Eng., C*, 2016, **68**, 241–250.

38 Q. Li, L. Liu, X.-X. Zhong, F.-B. Li, A. M. Asiri, K. A. Alamry, N.-Y. Zhu, W.-Y. Wong and H.-M. Qin, *J. Inorg. Organomet. Polym. Mater.*, 2017, **27**, 101–109.

39 S. Rahman, A. Arami-Niya, X. Yang, G. Xiao, G. Li and E. F. May, *Chem. Commun.*, 2020, **3**, 186.

40 S. Ehrling, E. M. Reynolds, V. Bon, I. Senkovska, T. E. Gorelik, J. D. Evans, M. Rauche, M. Mendt, M. S. Weiss, A. Pöppl, E. Brunner, U. Kaiser, A. L. Goodwin and S. Kaskel, *Nat. Chem.*, 2021, **13**, 568–574.

41 D. S. Laitar, P. Müller and J. P. Sadighi, *J. Am. Chem. Soc.*, 2005, **127**, 17196–17197.

42 S. Díez-González, E. D. Stevens, N. M. Scott, J. L. Petersen and S. P. Nolan, *Chem.–Eur. J.*, 2008, **14**, 158–168.

43 F. Lazreg, F. Nahra and C. S. J. Cazin, *Coord. Chem. Rev.*, 2015, **293–294**, 48–79.

44 R. Hamze, J. L. Peltier, D. Sylvinson, M. Jung, J. Cardenas, R. Haiges, M. Soleilhavoup, R. Jazzar, P. I. Djurovich, G. Bertrand and M. E. Thompson, *Science*, 2019, **363**, 601–606.

45 R. Hamze, R. Jazzar, M. Soleilhavoup, P. I. Djurovich, G. Bertrand and M. E. Thompson, *Chem. Commun.*, 2017, **53**, 9008–9011.

46 K. K. Manar, S. Chakrabortty, V. K. Porwal, D. Prakash, S. K. Thakur, A. R. Choudhury and S. Singh, *ChemistrySelect*, 2020, **5**, 9900–9907.

47 D. Parasar, N. B. Jayaratna, A. Muñoz-Castro, A. E. Conway, P. K. Mykhailiuk and H. V. R. Dias, *Dalton Trans.*, 2019, **48**, 6358–6371.

48 A. Kobayashi and M. Kato, *Chem. Lett.*, 2017, **46**, 154–162.

49 M. Hashimoto, S. Igawa, M. Yashima, I. Kawata, M. Hoshino and M. Osawa, *J. Am. Chem. Soc.*, 2011, **133**, 10348–10351.

50 T. D. Keene, D. Rankine, J. D. Evans, P. D. Southon, C. J. Kepert, J. B. Aitken, C. J. Sumby and C. J. Doonan, *Dalton Trans.*, 2013, **42**, 7871–7879.

51 M. W. Logan, S. Langevin and Z. Xia, *Sci. Rep.*, 2020, **10**, 1492.

52 W. M. Bloch, R. Babarao and M. L. Schneider, *Chem. Sci.*, 2020, **11**, 3664–3671.

53 T. McPhillips, S. McPhillips, H. Chiu, A. E. Cohen, A. M. Deacon, P. J. Ellis, E. Garman, A. Gonzalez, N. K. Sauter, R. P. Phizackerley, S. M. Soltis and P. Kuhn, *J. Synchrotron Radiat.*, 2002, **9**, 401–406.

54 G. M. Sheldrick, *Acta Crystallogr., Sect. C: Struct. Chem.*, 2015, **71**, 3–8.

55 C. Adamo and V. Barone, *J. Chem. Phys.*, 1999, **110**, 6158–6170.

56 F. Neese, *WIREs Computational Molecular Science*, 2012, **2**, 73–78.

57 F. Neese, *WIREs Computational Molecular Science*, 2018, **8**, e1327.

58 F. Weigend and R. Ahlrichs, *Phys. Chem. Chem. Phys.*, 2005, **7**, 3297–3305.

59 S. Grimme, S. Ehrlich and L. Goerigk, *J. Comput. Chem.*, 2011, **32**, 1456–1465.